Preparation of porous ceramic membranes from Sayong ball clay

Maisarah Mohamed Bazin, Norhayati Ahmad & Yuzo Nakamura

THE CERAMIC SOCIETY OF JAPAN

THE KOREAN CERAMIC SOCIETY

Taylor & Francis
Taylor & Francis Group

ARTICLE

OPEN ACCESS | Check for updates

Preparation of porous ceramic membranes from Sayong ball clay

Maisarah Mohamed Bazin[a], Norhayati Ahmad[b] and Yuzo Nakamura[c]

[a]Mechanical Engineering Section, Universiti Kuala Lumpur, Malaysia France Institute, Bandar Baru Bangi, Selangor, 43650, Malaysia; [b]Department of Materials, Manufacturing & Industrial Engineering, School of Mechanical Engineering, Faculty of Engineering, Universiti Teknologi Malaysia, Johor Bahru 81300, Johor, Malaysia; [c]Department of Mechanical Engineering, Kagoshima University, Kagoshima-shi, Kagoshima, JAPAN

ABSTRACT

A porous ceramic membrane for the nano-filtration range was fabricated from a mixture of ball clay and starch. Sayong ball clay powders were mixed with starch as a pore former and compacted under a pressure of 200 MPa. The mixture was sintered at temperatures ranging from 900°C to 1200°C. It was found that the porous structure and crystalline phase of the sintered membrane were greatly dependent on the sintering temperature. The membranes exhibited bulk density varying from 1.5 g/cm^3 to 1.9 g/cm^3, an apparent porosity ranging from 40.2% to 0.34%, an average pore size of 23.16 to 5.11 nm and flexural strength ranging from 1 to 21 MPa as the sintering temperature was increased. The pore size observed by SEM is much larger than these values, and these observed pores are believed to construct open channels that act as the main paths for filtration, as discuss later. The permeation flux greatly dependent on the trans-membrane pressure and sintering temperatures. The membrane synthesized at 1050°C displayed the optimum properties as a nanofiltration membrane with a bulk density of 1.6 g/cm^3, apparent porosity of 18%, pore size of 9.84 nm and flexural strength of 6 MPa.

1. Introduction

Membrane technology is a rapidly growing technology that can be used in a large number of separation processes. Although polymeric membranes are more widely used for water and gas separation applications, inorganic membranes are still in high demand since the separation industry requires membranes with good thermal, mechanical and chemical stability. Besides separation processes, ceramic membranes are also applicable in the food, beverage, biotechnological, pharmaceutical and electronic industries.

Various kinds of inorganic membrane materials are available on the market. Most of these membranes are developed from alumina, as reported in the literature [1–5]. However, the production of alumina-based membranes results in high costs because alumina is an expensive material that requires high sintering temperatures [6,7]. In order to reduce costs, recent research on fabrication of ceramic membranes focuses more on the utilization of cheaper natural raw materials such as kaolin [8–10], fly ash [11,12] and clay [4,6,7,13–15].

Clay is a mineral composed of hydrated aluminum silicates and other metal oxides such as Fe_2O_3, MgO and K_2O [16]. Clay bodies may undergo several changes during the firing process because of physical, chemical and mineralogical modifications. Various types of clay were studied as membrane materials and encouraging findings were obtained. Masturi et al. [16] succeeded in producing a ceramic filter using clay from Plered, Indonesia as the raw material. The coated membranes obtained by the sol-gel method with titania to induce photocatalytic activity to degrade pollutants. Sarkar et al. [4] developed porous capillary tubes using clay-alumina mixtures with different clay contents. The purpose of adding clay in this process is to achieve low cost while still producing mechanically strong capillary tubes. Palacio et al. [17] fabricated flat disk membranes from natural clay, and phosphate from Moroccan ores. They added starch as a pore former in their study.

The main objective of this work is to fabricate a porous ball clay membrane with high porosity and mechanical strength. An additional purpose is to reduce fabrication costs by using inexpensive, naturally occurring raw materials, with a low sintering temperature and simple fabrication technique. For these reasons, we selected Sayong ball clay, a representative cheap natural resource from Malaysia, with corn starch as pore-forming material during sintering. The effects of the sintering temperature on the microstructural properties of the membrane were characterized.

2. Experimental setup

2.1. Fabrication of membranes

The starting material was Sayong ball clay from Perak, Malaysia. The ball clay powder was sieved with a 75 μm

mesh standard screen and mixed with corn starch (Glow-San Sdn. Bhd.) in a mass ratio of 70:30. The mixtures then underwent a dry milling process using a Lab Roller Mixer-LRM 30 (China, 40 alumina balls) at 140 rpm for 5 hours. Corn starch served as a porosity agent for the membranes. The mixtures were pressed in stainless-steel molds with a universal testing machine under a pressure of 200 MPa to form circular disk-shaped green bodies measuring 30 mm in diameter and 2.5 mm in thickness. The samples were then sintered at seven different temperatures ranging from 900°C to 1200°C for a holding time of 2 hours in air. The heating and cooling rates were controlled at $\pm$ 5°C/min, respectively.

2.2. Characterization techniques

The chemical composition of the ball clay was confirmed by X-ray fluorescence (XRF) analysis (Philip, Model-PW2400, USA). Thermogravimetric (TGA) and differential thermal (DTA) analyzes were performed in air using a TGA/SDTA 851 Modul (Mettler Toledo, USA). In the TGA and DTA analyzes, the temperature was raised at 10°C/min from room temperature to 900°C. The particle size distribution of the mixture powders was measured with a particle size analyzer (Mastersizer, Malvern Instruments, UK).

X-ray diffraction (XRD) analysis of the powder and sintered membranes was conducted using a Bruker D8 Advance (Germany) machine and their microstructures were observed by field emission scanning electron microscopy (FESEM: Zeiss Supra 35VP, Germany). The average pore size was measured by nitrogen adsorption using Micromeritics ASAP 2020. The pore size distribution (PSD) was calculated according to the Barrett-Joyner-Halenda (BJH) method based on an adsorbent model comprising a collection of cylindrical pores, assuming a cylindrical, non-connecting pore geometry [18].

Density is an important physical property for understanding the densification of materials. On the other hand, porosity is one of the key factors determining the performance of membranes. The apparent porosity and bulk density of the membranes were measured by immersion test using an Analytical Balanced GR200 (USA), according to the ASTM C373-88 standard. The mass of the samples under dry condition (W_d) was measured first. Next, the samples were vacuumed in a desiccator filled with distilled water for a day to make sure that all the pores were filled with water. Then, the suspended mass (W_s) and the mass after the samples were filled with water in air (W_w) were measured.

Three point bending tests were conducted according to the ASTM C-1161-02c Standard. The rectangular bars were prepared by the same procedure as the disc membranes. Testing was performed on a series of at least five rectangular bars with a size of 80 mm x

30 mm x 2.5 mm to obtain the average strength for each series. The tests were conducted with a span of 40 mm under a crosshead speed of 0.5 mm/min with a tensile test machine (Instron 5982, US). The flexural strength indicated later was the average obtained for at least five specimens.

The performances of the membranes were tested by water filtration testing using a dead-end filtration system. The filtration process was conducted at room temperature. The pressure applied for the filtration process was 0.5 to 3 bars. A mass of 5 ml of permeate water was measured to calculate the water fluxes. Lake water was used as the wastewater source for the filtration process. It was assumed that the quality of the lake water was constant for the entire filtration processes. The pure water flux was measured using distilled water. The flux, J (kg/m^2.h), of permeate water was calculated according to the following equation:

$$\text{Flux}, J(\text{kg/m}^2.\text{h}) = \frac{m}{A\Delta t} \tag{1}$$

where m is the mass of filter water (kg), A is the surface area (m^2) and Δt t is the time in hours (h).

3. Results and discussion

3.1. Properties of Sayong ball clay

Table 1 shows the chemical composition of Sayong ball clay as determined by XRF analysis. Ball clay powders consist mainly of SiO$_2$ (51.28%) and Al$_2$O$_3$ (23.78%). The amount of alkaline oxides (K$_2$O and Na$_2$O) corresponds to about 3.41%. The presence of earth-alkaline elements (MgO and CaO) indicates that the clay is rich in carbonates [19].

Figure 1 presents XRD patterns of Sayong ball clay powder. The main phases present in the ball clay powder are quartz SiO$_2$, albite Na(AlSi$_3$O$_8$) and kaolinite Al$_2$(Si$_2$O$_5$)(OH)$_4$. It is clear from Figure 1 that the major crystalline phase is quartz.

Figure 2 shows profiles of the weight loss curves obtained from TGA and DTA analyzes of a ball clay and corn starch mixture. The initial weight of the sample was reduced by 15.84% when the temperature was increased to 500°C. This was due to the burning out of

Table 1. Chemical composition of the Sayong ball clay used in the present study.

Component	Wt %
SiO$_2$	51.28
Al$_2$O$_3$	23.78
Na$_2$0	2.07
K$_2$O	1.34
MgO	1.48
CaO	0.81
Fe$_2$O$_3$	0.46
TiO$_2$	0.36
P$_2$O$_5$	0.36
SO$_3$	0.06
Etc.	17.80
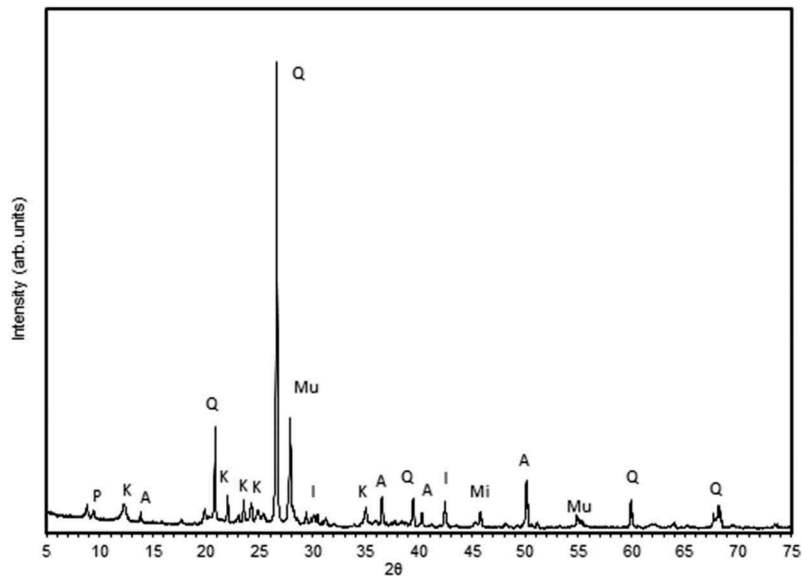
Figure 1. XRD diffractogram of ball clay powder [Q: quartz; A: albite; K: kaolinite; I: illite; Mi: microline; Mu; muscovite; P: potassium aluminum silicate].
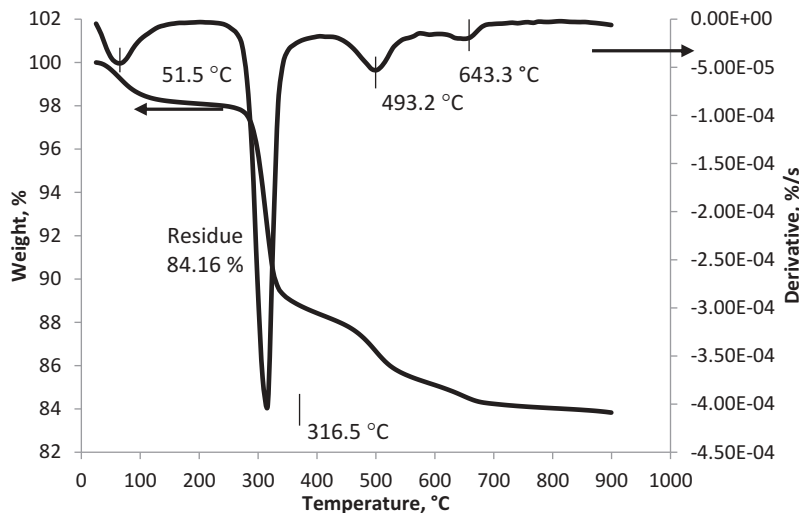
Figure 2. Thermogravimetric and differential thermal analyzes of raw clay and corn starch.

the organic additive (corn starch) from the paste and the removal of water from the clay. At a temperature of 643.3℃, dehydroxylation of the clay minerals occurred [4]. No additional peak was found above that temperature. At above 800℃, the mixture shows a slight weight loss. This result suggests that 800℃ is the lowest sintering temperature for obtaining stable sintering support.

Figure 3 shows the particle size distribution in the mixture of starch and ball clay powders. The average particle size of the mixture powder was 14.54 μm, and the sizes of 90% of the particles were less than 20 μm.

3.2. Properties of the ball clay membranes

Figure 4 shows XRD patterns of the specimens sintered at temperatures ranging from 900℃ to 1200℃. As in the powder, the main phase present in the sintered specimens is quartz. At 900℃, most of the phases present in

the powder remains after sintering. However, the intensity of the XRD peaks in all of the crystalline phases (albite, kaolinite, illite, microline and muscovite) decreased with increases in temperature. The XRD peaks of quartz as well as the other crystalline minerals began to decrease at above 1000℃, which suggests that these materials dissolve into the glass matrix. At 1200℃, only a small amount of the quartz phase remained. At lower sintering temperatures (900–1100℃), the formation of muscovite sometimes occurred due to the relatively high K_2O content. In such cases, the kaolinite phase disappeared due to the conversion of kaolinite to metakaolinite. These results suggested that the crystalline phases were transformed into amorphous phases, and that transformation was enhanced by the temperature.

The microstructures at the cross sections of ball clay membranes sintered at different temperatures are shown in Figure 5. The microstructure changed
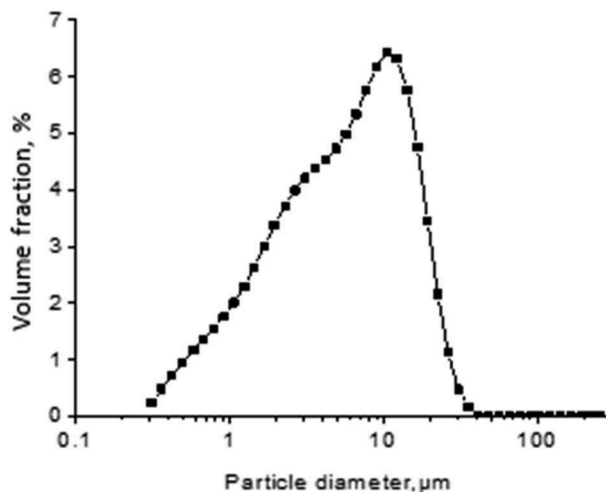
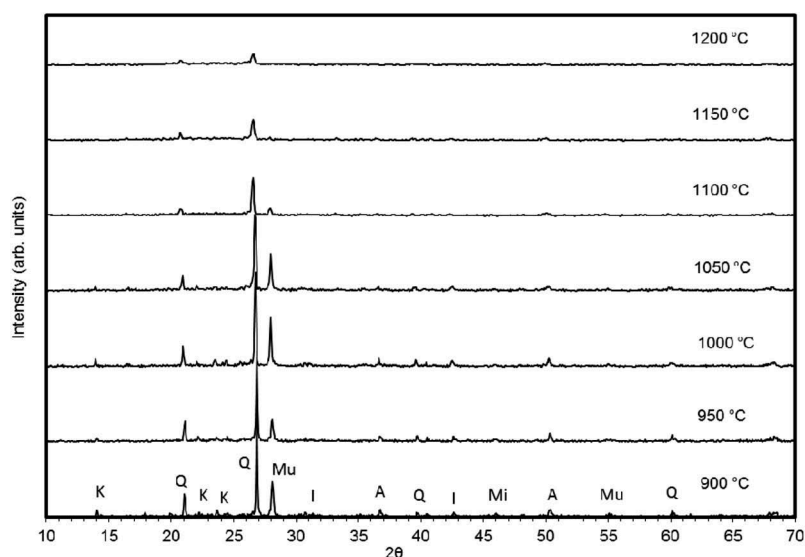**Figure 3.** Particle size distribution of the mixture powder.

Figure 4. XRD patterns of raw clay [Q: quartz; A: albite; K: kaolinite; I: illite; Mi: microline; Mu; muscovite].

with the sintering temperature. At 900°C, the surface of the membranes was rough and individual ball clay particles were clearly visible. Interconnected pores seem to have been formed at this temperature. At 1000°C, well-bonded particles rather than detached particles were seen. At 1150°C, the membrane body became denser and the open porosity had almost completely disappeared. Closed pores were formed at this temperature. Other studies [3,17] obtained similar results.

Changes in the pore size were observed further through microstructure analysis. A non-uniform pore size distribution was observed in the microstructures. At 900°C, the pore size was smaller. The pores became larger with increases in temperature. At a high sintering temperature (1200°C), the pores coalescenced, which lead to the development of these large pores. Some of the pores may even have disappeared at high temperatures. These results are in good agreement with those reported elsewhere [7,9,15,20–22]. According to Wei et

al. [23], high sintering temperatures caused increases in pore size, which they attributed to small pores connecting with each other.

Figure 6 shows the size distributions of mesoscopic pores in the sintered specimens obtained by the nitrogen adsorption method. Pore size was evaluated using the Kelvin equation, which describes the effect of the surface curvature of the liquid–vapor meniscus on the vapor pressure and relates the pore diameter to the relative pressure (P/P_0):

$$\ln \frac{P}{P_o} = \frac{2\gamma V \cos \theta}{RTr_m} \qquad (2)$$

where P is the actual vapor pressure, P_o is the saturated vapor pressure, γ is the surface tension, V is the molar volume of the liquid, R is the universal gas content, r is the radius of the droplets, and T is temperature.

All the membranes exhibited multimodal pore size distribution, which indicates the existence of more than two distinct or overlapping peaks [21]. The wide
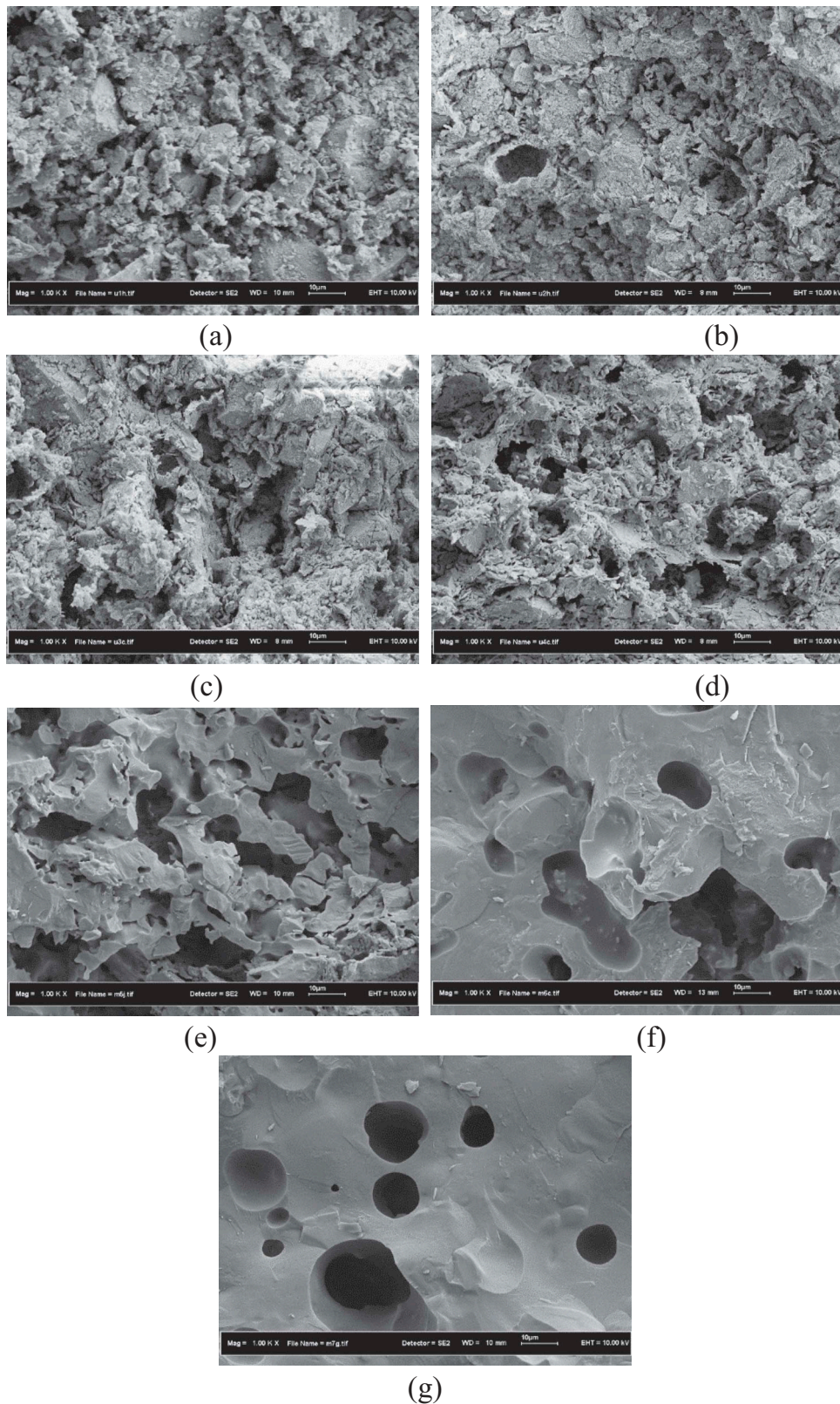
Figure 5. FESEM micrographs of a ball clay membrane at different temperatures: (a) 900℃; (b) 950℃; (c) 1000℃; (d) 1050℃; (e) 1100℃; (f) 1150℃; and (g) 1200℃.

distribution of the pore sizes resulted from the non-uniform pore shapes (Figure 5). The average pore diameters measured were 23.16, 12.8, 9.84 and 5.11 nm for 900, 1000, 1050 and 1100℃, respectively. More interconnected pores were formed at lower sintering temperatures. Adsorbed gas filled the interconnected pores and converted the pores to single pores. Thus, larger pore sizes were detected at 900℃.

Figure 7 shows the effect of sintering temperature on the apparent porosity and bulk density of the membranes. The apparent porosity was reduced and bulk density increased with increases in the temperature.
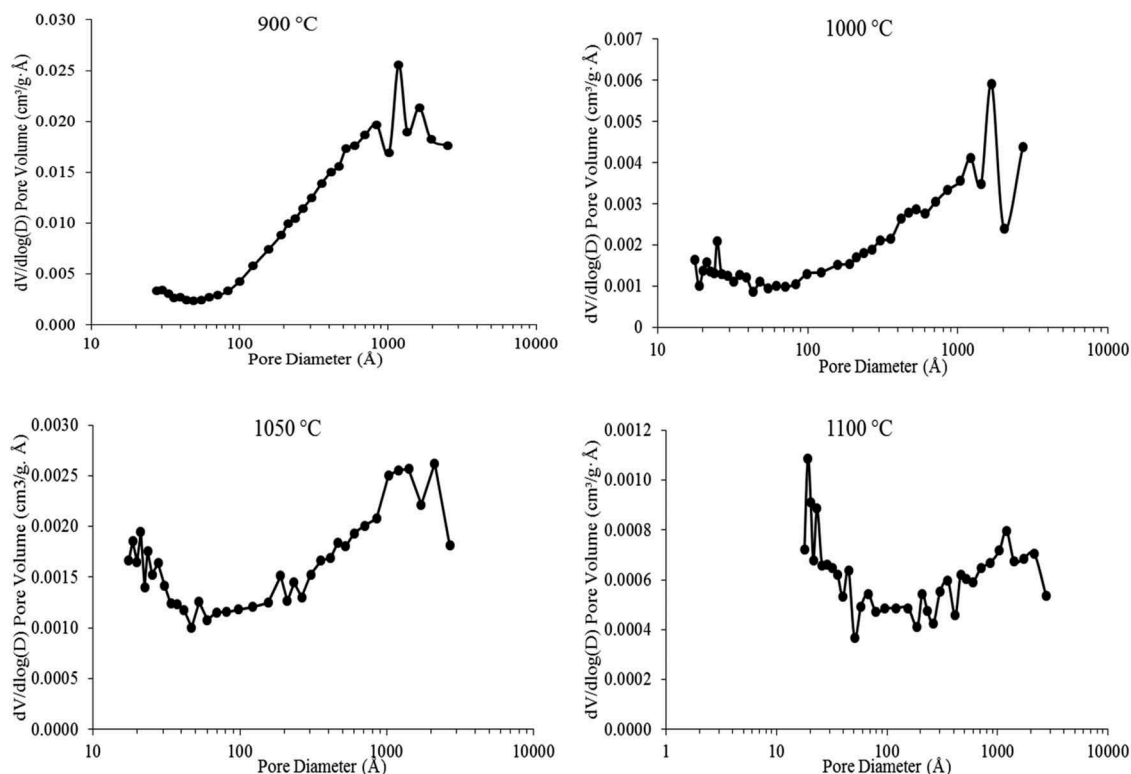
Figure 6. Pore size distributions of ball clay membranes at different sintering temperatures.
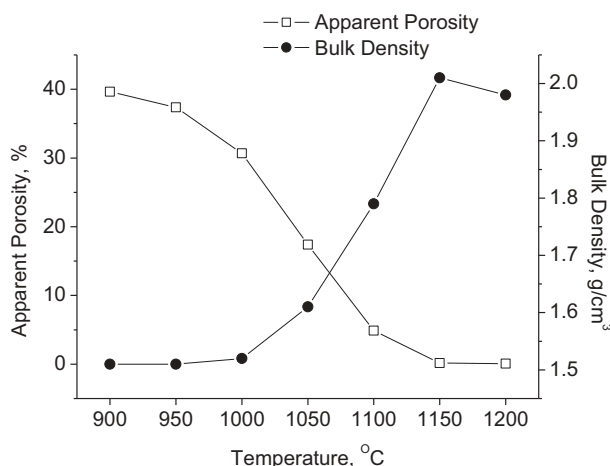

Figure 7. Effects of sintering temperatures on apparent porosity and bulk density.

The addition of starch during the fabrication process increased the porosity volume in the sintered bodies, as reported in the previous study [24]. In the first temperature range (900–1000°C), however, the densification was very slow. In the second temperature range from 1000°C to 1150°C, the density increased abruptly from 1.52 to 2.01 g/cm³ with increases in temperature. Most of the densification process occurred in this second temperature range. The apparent porosity was close to zero at 1150°C and 1200°C, where the density was saturated at about 2.0 g/cm³. The temperature boundary between first and second intervals (~1000°C) may be regarded as the glass transition temperature, above which sintering is caused by a viscous flow.

The presence of flux materials (K_2O, Na_2O and Fe_2O_3) led to formation of a glassy viscous phase and facilitated the densification process [25]. This glassy viscous phase penetrated the pores, closing them and isolating the neighboring pores. This caused densification of the sintered specimen and, at the same time, reduced the porosity [22]. The viscosity was lower at higher temperatures, which led in turns to a larger volume of the glassy phase. It is therefore to be expected that densification increases with increases in temperature [25].

The flexural strength of the membranes increased from 1 MPa to 21 MPa with increases in the sintering temperatures from 900°C to 1200°C, as shown in Figure 8. By comparing Figure 8 with Figure 7, it becomes clear that the increases in a strength with
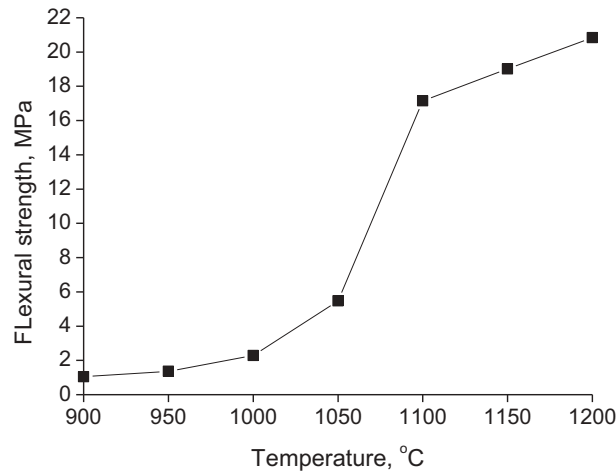
Figure 8. Flexural strength of membranes at different sintering temperatures.

the sintering temperature correspond to the increases in density as well as to the decreases in porosity. It can also be seen from Figure 5 that the increases in strength with temperature are closely related to changes in the microstructure. As the temperature is elevated, clay grains are refined and interconnected with each other. These microstructural features suggest that not only does the strength of each clay grain increase, but the bonding strength of neighboring grains also becomes greater, as the sintering temperature is elevated. Similar trends in the increase in the flexural strength with sintering temperatures were observed by other authors [7,10,15,26,27]. These results indicate that the optimum temperatures for obtaining stable sintered specimens are above 800° C. Below this temperature, the sintered specimens are extremely brittle.

The variations in fluxes with transmembrane pressure from 0.5 to 3 bars are shown in Figure 9 and Figure 10. Overall, the initial pure water flux was higher than the flux of lake water. The flux increased proportionally with increases in transmembrane pressure. Vasanth et al. [7] reported that increasing the driving force with pressure across the membrane caused the flux to rise. The linear

relationship between the flux and the transmembrane pressure indicates that the driving force for solvent permeation is the pressure difference. Filtration testing using lake water showed that the values of the permeate fluxes for all the membranes were reduced from those of the initial pure water fluxes (Figure 9). The presence of particulates in lake water may reduce the permeate flux. The concentration of polarization formed on the membrane surface becomes the resistance that reduces the fluxes.

4. Conclusions

Porous ceramic membranes with considerably good strength were successfully fabricated from Sayong ball clay using a simple uniaxial compaction method. The sintering temperature has a significant effect on the microstructure of the membranes, encouraging production of a high-strength structure with optimum porosity. Findings indicate that the porosity and strength of the membranes can be controlled by varying the sintering temperature. The fluxes for both pure and wastewater increase with the transmembrane pressure and are higher, on average, for membranes sintered at higher
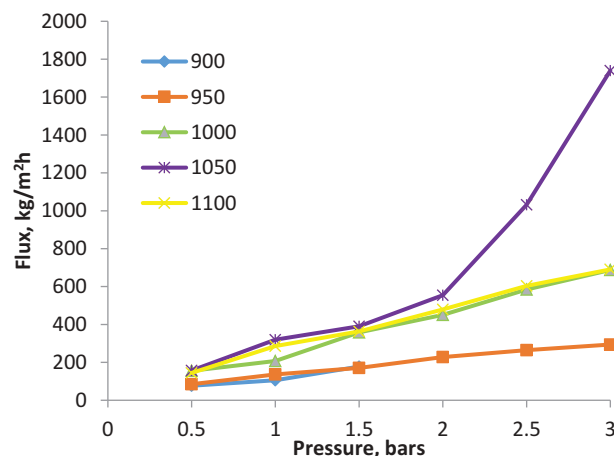
Figure 9. Variations in pure water fluxes at different transmembrane pressures.
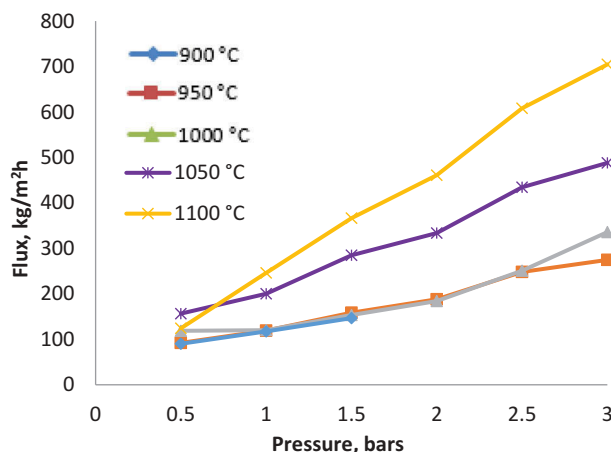
Figure 10. Variations in wastewater fluxes at different transmembrane pressures.

sintering temperatures. Sintering at 1050°C produces membranes with optimum strength (6 MPa) and porosity (18%) and was thus considered to be the best sintering temperature for fabrication of Sayong ball clay membranes.

Disclosure statement

No potential conflict of interest was reported by the authors.

Funding

References

[1] Cortalezzi MM, Rose J, Barron AR, et al. Characteristics of ultrafiltration ceramic membranes derived from alumoxane nanoparticles. J Membr Sci. 2002;205:33–43.

[2] Yoshino Y, Suzuki T, Nair BN, et al. Development of tubular substrates, silica based membranes and membrane modules for hydrogen separation at high temperature. J Membr Sci. 2005;267:8–17.

[3] Yang GCC, Tsai CM. Effects of starch addition on characteristics of tubular porous ceramic membrane substrates. Desalination. 2008;233:129–136.

[4] Sarkar S, Bandyopadhyay S, Larbot A, et al. New clay-alumina porous capillary supports for filtration application. J Membr Sci. 2012;392–393:130–136.

[5] Li S, Wang CA, Zhou J. Effect of starch addition on microstructure and properties of highly porous alumina ceramics. Ceram Int. 2013;39:8833–8839.

[6] Mecif A, Soro J, Harabi A, et al. Preparation of Mullite- and Zircon-based ceramics using kaolinite and zirconium oxide: a sintering study. J Am Ceram Soc. 2010;93:1306–1312.

[7] Vasanth D, Uppaluri R, Pugazhenthi G. Influence of sintering temperature on the properties of porous ceramic support prepared by uniaxial dry compaction method using low-cost raw materials for membrane applications. Sep Sci Technol. 2011;46:1241–1249.

[8] Kazemimoghadam M, Pak A, Mohammadi T. Dehydration of water/1-1-dimethylhydrazine mixtures by zeolite membranes. Microporous Mesoporous Mater. 2004;70:127–134.

[9] Bouzerara F, Harabi A, Achour S, et al. Porous ceramic supports for membrane prepared from kaolin and doloma mixtures. J Eur Ceram Soc. 2006;26:1663–1671.

[10] Nandi BK, Uppaluri R, Purkait MK. Preparation and characterization of low cost ceramic membranes for microfiltration applications. Appl Clay Sci. 2008;42:102–110.

[11] Fang J, Qin G, Wei W, et al. Preparation and characterization of tubular supported ceramic microfiltration membranes from fly ash. Sep Purif Technol. 2011;80:585–591.

[12] Jedidi I, Khemakhem S, Saidi S, et al. Preparation of new ceramic microfiltration membrane from mineral coal fly ash: application to the treatment of the textile dying effluents. Powder Technol. 2011;208:427–432.

[13] Bentama J, Ouazzani K, Elgarouani A. New membranes made of sintered clay application to cross-flow microfiltration. Afr J Sci Technol. 2003;4:38–41.

[14] Khemakhem S, Larbot A, Amar RB. New ceramic microfiltration membranes from Tunisian natural materials: application for the cuttlefish effluents treatment. Ceram Int. 2009;35:55–61.

[15] Monash P, Pugazhenthi G. Development of ceramic supports derived from low-cost raw materials for membrane applications and its optimization based on sintering temperature. Int J Appl Ceram Technol. 2011;8(1):227–238.

[16] Masturi S, Aji MP, Sustini E, et al. Permeability, strength and filtration performance for uncoated and titania-coated clay wastewater filters. Am J Environ Sci. 2012;8:79–94.

[17] Palacio L, Bouzerdi Y, Ouammou M, et al. Ceramic membranes from moroccan natural clay and phosphate for industrial water treatment. Desalination. 2009;245:501–507.

[18] Kuila U Measurement and interpretation of porosity and pore-size distribution in mudrocks: the hole story of shales [dissertation]. Colorado School of Mines; 2013.

[19] Baccour H, Medhioub M, Jamoussi F, et al. Influence of firing temperature on the ceramic properties of Triassic clays from Tunisia. J Mater Process Technol. 2009;209:2812–2817.

[20] Mosadeghkhah A, Alaee MA, Mohammadi T. Effect of sintering temperature and dwell time and pressing pressure on Ba0.5Sr0.5Co0.8Fe0.2O3-δ perovskite-type membranes. Mater Des. 2007;28:1699–1706.

[21] Bouzerara F, Harabi A, Condom S. Porous ceramic membranes prepared from kaolin. Desalin Water Treat. 2009;12:415–419.

[22] Das B, Chakrabarty B, Barkakati P. Preparation and characterization of novel ceramic membranes for micro-filtration applications. Ceram Int. 2016;42:14326–14333.

[23] Wei Z, Hou J, Zhu Z. High-aluminum fly ash recycling for fabrication of cost-effective ceramic membrane supports. J Alloys Compd. 2016;683:474–480.

[24] Maisarah MB, Muhd Amirudin A, Nurhanna Z, et al. Effect of starch addition on microstructure and strength of ball clay membrane. J Teknol. 2014;69:117–120.

[25] Milheiro FAC, Freire MN, Silva AGP, et al. Densification behaviour of a red firing Brazilian Kaolinitic clay. Ceram Int. 2005;31(5):757–763.

[26] Saffaj N, Persin M, Younsi SA, et al. Elaboration and characterization of microfiltration and ultrafiltration membranes deposited on raw support prepared from natural Moroccan clay: application to filtration of solution containing dyes and salts. Appl Clay Sci. 2006;31:110–119.

[27] Khemakhem M, Khamekhem S, Ayedi S, et al. Study of ceramic ultrafiltration support based on phosphate industry subproduct: application for the cuttlefish conditioning effluents treatment. Ceram Int. 2011;37:3617–3625.